The Astrophysical Journal Supplement Series, 283:73 (14pp), 2026 April https://doi.org/10.3847/1538-4365/ae4b3f

Probing Departures from ΛCDM by Late-time Datasets

Himanshu Chaudhary[1,2], Vipin Kumar Sharma[3,4], Salvatore Capozziello[5,6,7], and G. Mustafa[8,9,10]
[1] Department of Physics, Babeş-Bolyai University, Kogălniceanu Street, Cluj-Napoca 400084, Romania; himanshu.chaudhary@ubbcluj.ro, himanshuch1729@gmail.com
[2] Research Center of Astrophysics and Cosmology, Khazar University, Baku, AZ1096, 41 Mehseti Street, Azerbaijan
[3] Indian Institute of Astrophysics, Koramangala II Block, Bangalore 560034, India; vipinkumar.sharma@iiap.res.in
[4] International Center for High Energy Physics and Applications, Lovely Professional University, Phagwara, Punjab, 144411, India
[5] Dipartimento di Fisica "E. Pancini," Università di Napoli "Federico II," Complesso Universitario di Monte Sant' Angelo, Edificio G, Via Cinthia, I-80126 Napoli, Italy; capozziello@na.infn.it
[6] Istituto Nazionale di Fisica Nucleare (INFN), sez. di Napoli, Via Cinthia 9, I-80126 Napoli, Italy
[7] Scuola Superiore Meridionale, Largo S. Marcellino, I-80138 Napoli, Italy
[8] Department of Physics, Zhejiang Normal University, Jinhua 321004, People's Republic of China; gmustafa3828@gmail.com
[9] Zhejiang Institute of Photoelectronics and Zhejiang Institute for Advanced Light Source, Zhejiang Normal University, Jinhua, Zhejiang 321004, People's Republic of China
Received 2025 October 19; revised 2026 February 15; accepted 2026 February 25; published 2026 March 30

Abstract

Observational data play a pivotal role in identifying cosmological models that are both theoretically consistent and empirically viable. In this work, we investigate the level of preference for dynamical dark energy over a cosmological constant using current late-time observational datasets, including cosmic chronometers (CC), baryon acoustic oscillations from Dark Energy Spectroscopic Instrument (DESI) DR2, and different Type Ia supernova catalogs (Pantheon$^+$, DES-Dovekie, Union3). We analyze various dynamical dark-energy models, including ωCDM, oωCDM, $\omega_0\omega_a$CDM, logarithmic, exponential, Jassal–Bagla–Padmanabhan (JBP), Barboza–Alcaniz (BA), and GEDE. In most cases, the oΛCDM and oωCDM models favor an open Universe. For the oωCDM, the inclusion of DES-Dovekie or Union3 data together with CC and DESI DR2 favors a nearly flat geometry. Using the CC + DESI DR2 dataset, the preference for dynamical dark energy lies between the 1σ and 2σ level. When different supernova catalogs (DES-Dovekie or Union3) are included, the deviation from ΛCDM in the ωCDM, $\omega_0\omega_a$CDM, logarithmic, JBP, BA, and GEDE models increases to the 2σ–2.74σ level, while the Pantheon$^+$ sample yields deviations below the 2σ level. We find consistent evidence for $\omega_0 > -1$ and $\omega_a < 0$ across all dark-energy models, indicating a preference for dynamical dark energy characterized by a Quintom-B-type scenario. The ΛCDM paradigm has long served as the standard framework of modern cosmology; however, recent DESI DR2 results have exposed emerging tensions with the cosmological constant Λ, hinting at possible new physics in the dark-energy sector. Even so, the currently available data are still not strong enough to definitively rule out the ΛCDM model.

Unified Astronomy Thesaurus concepts: Cosmological parameters (339)

1. Introduction

The late-time accelerated expansion of the Universe remains one of the most profound mysteries in modern cosmology (A. G. Riess et al. 1998; S. Perlmutter et al. 1999). Within the standard Lambda cold dark matter (ΛCDM) framework, this phenomenon is attributed to a positive cosmological constant Λ with negative pressure, introduced in Einstein's field equations of general relativity (A. Einstein 1917). Although ΛCDM provides an excellent fit to observational data, the cosmological constant itself is a phenomenological parameter lacking a fundamental theoretical explanation for its observed value (Y. B. Zel'dovich 1968; S. Weinberg 1987; S. Weinberg 1989). Furthermore, the magnitude of Λ required by current observations implies a cosmic coincidence, marking our epoch as a particularly special time in the evolution of the Universe (S. Weinberg 1989; S. M. Carroll 2001; T. Padmanabhan 2003). In response to these conceptual challenges, numerous theoretical models have been proposed to explain cosmic acceleration through dynamical mechanisms (S. M. Carroll 2001; M. Chevallier & D. Polarski 2001; E. V. Linder 2003; V. Sahni & A. Starobinsky 2006; J. A. Frieman et al. 2008; A. De Felice & S. Tsujikawa 2010; T. P. Sotiriou & V. Faraoni 2010; S. Capozziello & M. De Laurentis 2011; M. Li et al. 2011; S. Nojiri et al. 2017; M. Benetti & S. Capozziello 2019; E. Piedipalumbo et al. 2023; C.-G. Park et al. 2025; G. Guin et al. 2025). These alternative scenarios usually feature dynamical energy densities that effectively reproduce the behavior of Λ. To explore the variety of possible models, we adopt parameterizations of cosmological quantities at the background level. This includes models involving expansions, parameterizations, or principal component analyses of the equation of state (EoS) $w \equiv p/\rho$ of a dark-energy fluid with the pressure p and energy density ρ (E. V. Linder 1988; M. Chevallier & D. Polarski 2001; E. V. Linder 2003; C.-G. Park et al. 2025).

In modern concordance cosmology, there are certain discrepancies attributed to datasets (for instance, the Hubble H_0—about $>4\sigma$—and S8 $=\sigma_8\sqrt{\Omega_m/0.3}$—about 2σ–3σ—parameter measurements; S. Basilakos & S. Nesseris 2017; T. M. C. Abbott et al. 2018; S. Joudaki et al. 2018; E. Di Valentino 2021). The full-shape analyses of large-scale

[10] Corresponding author.

structure data indicate a more pronounced tension, reaching a significance level of at least 4.5σ (S.-F. Chen et al. 2024; M. M. Ivanov et al. 2025), thereby suggesting a potential inconsistency between constraints derived from early and late-time observations of the Universe.

Complementing these findings, early results from Planck 2013 (P. A. R. Ade et al. 2014) suggested $\omega = -1.13^{+0.13}_{-0.14}$, slightly favoring the phantom regime. Using subsequent improvements in supernova (SN) calibration, in 2014 the Joint Light-curve Analysis (JLA) dataset (M. Betoule et al. 2014) reduced this discrepancy, and combining JLA with Planck 2013 brought dark-energy constraints in agreement with ΛCDM. Planck 2015 (P. A. R. Ade et al. 2016), using JLA as its default SN dataset, confirmed this consistency, yielding $\omega = -1.006^{+0.085}_{-0.091}$. However, in 2022, the Pantheon$^+$ SN compilation (D. Brout et al. 2022) reported $\omega = -0.90 \pm 0.14$ (SN only), and $\omega = -0.978^{+0.024}_{-0.031}$ when combined with cosmic microwave background (CMB) and baryon acoustic oscillation (BAO) data, consistent with ΛCDM within 2σ. The Union3 compilation by D. Rubin et al. (2025) further supported this trend, indicating mild tension with ΛCDM at 1.7σ–2.6σ and favoring dynamical dark-energy models with $\omega_0 > -1$ and $\omega_a < 0$.

Furthermore, in 2024, building on hints from the Pantheon$^+$ and Union3 catalogs, DESY5 found that best-fit values of ω were consistently slightly greater than -1 at more than the 1σ level, both for SN data alone and combined with CMB, BAO, and 3×2 pt measurements, supporting a trend toward mildly dynamical dark energy. The Dark Energy Spectroscopic Instrument (DESI)'s first-year BAO data (A. Adame et al. 2025) further strengthened this evidence, showing deviations from ΛCDM at 2.6σ–3.9σ when combined with CMB, Pantheon+, Union3, and DESY5 datasets, favoring a dynamical dark-energy scenario with $\omega_0 > -1$, $\omega_a < 0$, and $\omega_\omega + \omega_a < -1$ (Quintom-B). DESI Data Release 2 (DR2) BAO data (M. A. Karim et al. 2025) alone exclude ΛCDM at 3.1σ, and up to 4.2σ when combined with other datasets, with improved precision over DR1.

In the DESI DR2 analysis, the combination of DESI DR2 + CMB + DES-SN5Y leads to a preference for dynamical dark energy at the 4.2σ level, which is significantly stronger than that obtained using other SNe Ia samples. This striking result has motivated several recent studies (H. Chaudhary et al. 2025b; M. Cortês & A. R. Liddle 2025; G. Efstathiou 2025; I. D. Gialamas et al. 2025; S. Capozziello et al. 2026) to investigate the origin of this preference. These works have shown that 194 SNe Ia in the DES-SN5Y sample lie at very low redshift ($z < 0.01$) and are primarily responsible for the apparent preference for dynamical dark energy. When these low-z SNe Ia are excluded from the analysis, the consistency with the standard ΛCDM model is largely restored. These results show the possibility of systematic effects in the DES-SN5Y sample. Indeed, L. Huang et al. (2025) showed, using a systematic diagnosis, that there is an offset of approximately 0.043 mag between the low-z and high-z subsets of the DES-SN5Y sample. The Dark Energy Survey (DES) Collaboration recently reported improved cosmological constraints from a reanalysis of the DES-SN5Y dataset, showing that the preference for dynamical dark energy persists but with a reduced statistical significance of 3.2σ, compared to the earlier 4.2σ result obtained with DES-SN5Y (B. Popovic et al. 2025). These discrepancies have inspired extensive investigations into the underlying new physics and its fundamental nature, leading to the development of a wide range of models that describe dark energy as a dynamical phenomenon (S. Vagnozzi 2020, 2023; S. Roy Choudhury & T. Okumura 2024; J.-Q. Jiang et al. 2024; S. Barua & S. Desai 2025; S. Roy Choudhury 2025; S. Roy Choudhury et al. 2025; E. Fazzari et al. 2025; S. Lee 2025, 2026; T. Liu et al. 2025; R. Mazumdar et al. 2025; D. Pedrotti et al. 2026).

The persistent discrepancies observed across multiple cosmological datasets call into question the completeness of the ΛCDM model, potentially motivating refinements in modeling techniques or extensions to its theoretical foundation. A model-independent approach to probing such deviations involves the parameterization of the dark EoS, $\omega(z)$. This study considers different parameterizations of the EoS, based on the Chevallier–Polarski–Linder (CPL) form (M. Chevallier & D. Polarski 2001), also known as parameterization $\omega_0\omega_a$. The CPL framework enables the investigation of deviations from a true cosmological constant, and when applied to combined analyses of CMB data and various Type Ia supernova (SN Ia) datasets, it reveals a departure from $\omega = -1$.

In this paper, we go beyond the standard CPL parameterization and consider a broad and extended class of dark-energy models, including ωCDM, CPL, logarithmic, exponential, Barboza–Alcaniz (BA), Jassal–Bagla–Padmanabhan (JBP), and GDED. While several recent studies have presented cosmological constraints using DESI DR2 data in combination with external probes, most notably CMB measurements (K. Lodha et al. 2025a, 2025b; T.-N. Li et al. 2026), the present work is deliberately designed to test the preference for dynamically evolving dark energy over the ΛCDM model using only *late-time* observables. This approach allows us to test the preference for dynamical dark-energy models in the absence of assumptions tied to early Universe physics and to examine whether the preference for dynamical dark energy persists once CMB information is excluded. During our analysis, we focus on DESI DR2 BAO measurements combined with cosmic chronometers (CC) and three independent Type Ia SN samples (Pantheon$^+$, DES-Dovekie, and Union3). Our paper is organized as follows. In Section 2, we introduce the cosmological background equations and models. Section 3 details the core of this work with datasets and methodology using the Markov Chain Monte Carlo (MCMC) sampling against the recent DESI DR2 dataset, while Section 4 is dedicated to the discussion of results. In Section 5, we draw the conclusions.

2. The Background Cosmology

Under the two foundational conditions, i.e., spatial uniformity and directional symmetry of the cosmological principle, which has become a testable hypothesis supported by extensive observational evidence across cosmic scales (e.g., M. I. Scrimgeour et al. 2012; P. Laurent et al. 2016), the spacetime geometry of the Universe can be described by the Friedmann–Lemaître–Robertson–Walker (FLRW) spacetime metric,

$$ds^2 = dt^2 - a^2(t)\left[\frac{dr^2}{1 - kr^2} + r^2(d\theta^2 + \sin^2\theta\, d\phi^2)\right], \quad (1)$$

where r, θ, and ϕ denote the comoving spatial coordinates, and t represents cosmic time. The parameter k characterizes the spatial curvature of the 3D geometry of the Universe. The

Table 1
Dark-energy Parameterizations with Their Equations of State $\omega(z)$ and Evolution Functions $f_{\rm DE}(z)$

Parameterization	$\omega(z)$	$f_{\rm DE}(z)$	References
$\omega_0\omega_a$CDM	$\omega_0 + \frac{z}{1+z}\omega_a$	$(1+z)^{3(1+\omega_0+\omega_a)}e^{-\frac{3\omega_a z}{1+z}}$	(M. Chevallier & D. Polarski 2001; E. V. Linder 2003)
Logarithmic	$\omega_0 + \omega_a \log(1+z)$	$(1+z)^{3(1+\omega_0)}e^{\frac{3}{2}\omega_a(\log(1+z))^2}$	(G. Efstathiou 1999; R. Silva et al. 2012)
Exponential	$\omega_0 + \omega_a(e^{\frac{z}{1+z}} - 1)$	$e^{\left[3\omega_a\left(\frac{-z}{1+z}\right)\right]}(1+z)^{3(1+\omega_0+\omega_a)}e^{\left[3\omega_a\left(\frac{1}{4(1+z)^2}+\frac{1}{2(1+z)}-\frac{3}{4}\right)\right]}(1+z)^{\frac{3}{2}\omega_a}$	(M. Najafi et al. 2024)
JBP	$\omega_0 + \frac{z}{(1+z)^2}\omega_a$	$(1+z)^{3(1+\omega_0)}e^{\frac{3\omega_a z^2}{2(1+z)^2}}$	(H. Jassal et al. 2005)
BA	$\omega_0 + \frac{z(1+z)}{1+z^2}\omega_a$	$(1+z)^{3(1+\omega_0)}(1+z^2)^{\frac{3\omega_a}{2}}$	(E. Barboza & J. Alcaniz 2008)
GEDE	$-1 - \frac{\Delta}{3\ln(10)}\left[1+\tanh\left(\Delta\log_{10}\left(\frac{1+z}{1+z_t}\right)\right)\right]$	$\left(\frac{1-\tanh\left(\Delta\times\log_{10}\left(\frac{1+z}{1+z_t}\right)\right)}{1+\tanh(\Delta\times\log_{10}(1+z_t))}\right)$	(X. Li & A. Shafieloo 2020; V. K. Sharma et al. 2026)

evolution of the Universe is governed by the scale factor $a(t)$, which is a function of the energy densities and pressures of the components that fill the Universe. This time, evolution is formally governed by the two Friedmann equations, which follow from the Einstein field equations

$$R_{\mu\nu} - \frac{1}{2}Rg_{\mu\nu} = 8\pi G\left(T_{\mu\nu} - \frac{\Lambda}{8\pi G}g_{\mu\nu}\right) \quad (2)$$

when applied to an FLRW spacetime:

$$H^2 \equiv \left(\frac{\dot{a}}{a}\right)^2 = \frac{8\pi G}{3}\rho_i - \frac{k}{a^2} + \frac{\Lambda}{3}, \quad (3)$$

$$\frac{\ddot{a}}{a} = -\frac{4\pi G}{3}(\rho_i + 3p_i) + \frac{\Lambda}{3}. \quad (4)$$

Here, H denotes the Hubble expansion rate, Λ represents the cosmological constant, ρ_i is the aggregate energy density of all cosmic components, and p_i is the corresponding pressure. Although the cosmological constant Λ can be absorbed into the overall energy density, it is conventionally kept explicit to honor its historical introduction in Einstein's equations. In light of observations that confirm cosmic acceleration, Λ is now interpreted as the simplest form of dark energy.

Dark energy influences the expansion rate through two primary quantities: its current density parameter relative to the critical density, $\Omega_{\rm de}$, and its EoS parameter, ω. The most straightforward assumption is that the EoS parameter remains fixed in time. However, in the general case, ω may vary with cosmic time or redshift. The energy-momentum conservation equation,

$$\dot{\rho_i} + 3H\,(\rho_i + p_i) = 0, \quad (5)$$

is not independent but follows directly from combining Equations (3) and (4). Substituting the solution of Equation (5) that represents the redshift evolution of the individual energy components into Equation (3) yields the Hubble expansion function, which governs the dynamical evolution of the Universe:

$$E(z) = [\,\Omega_r(1+z)^4 + \Omega_m(1+z)^3 + \Omega_k(1+z)^2 + \Omega_\Lambda f_{\rm DE}(z)], \quad (6)$$

where $E(z) \equiv H^2(z)/H_0^2$ is the dimensionless Hubble function, H_0 is the present-day Hubble constant, and Ω_r, $\Omega_m = \Omega_b + \Omega_{\rm cdm}$, Ω_k, and Ω_Λ are the density parameters of radiation, matter (baryonic plus CDM), spatial curvature, and dark energy, respectively. Also, the function $f_{\rm DE}(z)$ denotes the redshift dependence of the dark-energy component and is defined as

$$f_{\rm DE}\,(\equiv\rho_{\rm DE}(z)/\rho_{\rm DE,0}) = \exp\left[3\int_0^z \frac{1+\omega(z')}{1+z'}\,dz'\right]. \quad (7)$$

For a cosmological constant ($\omega = -1$), $f_{\rm DE}(z) = 1$, and Equation (6) reduces to the standard oΛCDM,

$$E(z) = [\Omega_r(1+z)^4 + \Omega_m(1+z)^3 + \Omega_k(1+z)^2 + \Omega_\Lambda]. \quad (8)$$

In the special case of a spatially flat Universe ($\Omega_{k0} = 0$), Equation (8) reduces to

$$E(z) = [\,\Omega_r(1+z)^4 + \Omega_m(1+z)^3 + \Omega_\Lambda\,]. \quad (9)$$

In the case of a constant ω, Equation (7) simplifies to $(1+z)^{3(1+\omega)}$, and substituting this into Equation (6) yields the corresponding Hubble function of the oωCDM model.

$$E(z) = [\Omega_r(1+z)^4 + \Omega_m(1+z)^3 + \Omega_k(1+z)^2 + \Omega_\Lambda(1+z)^{3(1+\omega)}]. \quad (10)$$

Taking into account $\Omega_{k0} = 0$ in Equation (10), it reduces to the spatially flat ωCDM model.

$$E(z) = [\Omega_r(1+z)^4 + \Omega_m(1+z)^3 + \Omega_\Lambda(1+z)^{3(1+\omega)}]. \quad (11)$$

We also consider several dynamical dark-energy models that correspond to different functional forms of $\omega(z)$, as summarized in Table 1 (second column). For each model, using Equation (7), we can derive the corresponding form of $f_{\rm DE}(z)$ (third column). These expressions for $f_{\rm DE}(z)$ can then be substituted in Equation (6) to obtain the corresponding Hubble function, which characterizes the expansion history for each model.

3. Datasets and Methodology

In our analysis, we use the `SimpleMC`[11] cosmological inference code to estimate the posterior distributions of parameters for each cosmological model. In this code, we use the Metropolis Hastings MCMC algorithm (W. K. Hastings 1970), which allows efficient exploration of the parameter space. The

[11] https://github.com/ja-vazquez/SimpleMC

convergence of Markov Chains is tested using the Gelman–Rubin diagnostic ($R-1$) (A. Gelman & D. B. Rubin 1992), applying a strict threshold of $R-1<0.01$. The MCMC results are subsequently analyzed and visualized using the `GetDist` package (A. Lewis 2025). In our analysis, we used multiple datasets, with a focus on late-time observations, to determine the posterior distributions of the model parameters. The details of these datasets are provided below.

1. *Cosmic chronometers.* First, we consider CC, massive, passively evolving galaxies with old stellar populations and negligible star formation, which allow direct measurements of the Hubble parameter $H(z)$ via the differential age technique (R. Jimenez & A. Loeb 2002). These measurements are valuable for model-independent studies of the Universe's expansion history. For our analysis, we use 15 measurements from M. Moresco et al. (2012), M. Moresco (2015), and M. Moresco et al. (2016) instead of the 31 considered in S. Vagnozzi et al. (2021), as only these consist of statistical and systematic parts of the covariance matrix (M. Moresco et al. 2018, 2020). While S. Vagnozzi et al. (2021) consider only the statistical part.
2. *Baryon acoustic oscillations.* Next, we use recent BAO measurements from over 14 million galaxies and quasars (QSO) obtained by the DESI DR2 (M. A. Karim et al. 2025). These measurements are obtained from different tracers, such as the Bright Galaxy Sample, luminous red galaxies (LRG1), LRG2, LRG3+emission-line galaxies (ELG1), ELG2, QSO, and Lyα forests; for further details, see Section 3 of M. A. Karim et al. (2025). Each tracer provides different BAO measurements expressed through various ratios: D_M/r_d, D_H/r_d, D_V/r_d, and D_M/D_H. Here, $D_H(z)=c/H(z)$ represents the Hubble distance, $D_M(z)=c\int_0^z \frac{dz'}{H(z')}$ represents the comoving angular diameter distance, and $D_V(z)\equiv[zD_M^2(z)D_H(z)]^{1/3}$ represents the volume-averaged distance. The r_d corresponds to the sound horizon in the drag epoch, which in a flat ΛCDM model takes the value $r_d=147.09\pm0.2$ Mpc (N. Aghanim et al. 2020).
3. *Type Ia supernovae.* Finally, we use three different SN catalogs. First, we consider the Pantheon$^+$ sample (D. Brout et al. 2022), which comprises 1701 light curves from 1550 SNe Ia. In our analysis, we exclude the light curves below $z<0.01$, as these light curves are significantly affected by systematic uncertainties arising from peculiar velocities. Next, we use the recalibrated 1820 photometric SNe Ia light curves obtained over 5 yr by the Dark Energy Survey Supernova Program (DES-Dovekie; B. Popovic et al. 2025). This catalog consists of 1623 DES SNe Ia, with 197 low-redshift ($z<0.1$) SNe Ia from the CfA3-4/CSP Foundation sample (M. Hicken et al. 2009, 2012; R. Foley et al. 2018). The revised DES-Dovekie has 1718 SNe Ia overlapping between DES-Dovekie and DES SN5YR (T. M. C. Abbott et al. 2024). Finally, we use the Union3 compilation (D. Rubin et al. 2025), which comprises 2087 SNe Ia, including 1363 events overlapping with the Pantheon$^+$ sample. For each sample, we marginalize the parameter $\mathcal{M}$; see Equations (A9)–(A12) in M. Goliath et al. (2001) for further details.

To evaluate and compare the statistical performance of each model, we compute the Bayesian evidence $\ln\mathcal{Z}$ using the MCEvidence framework (A. Heavens et al. 2017). This metric quantifies the goodness of fit while penalizing the complexity of the model. The model comparison is performed via the Bayes factor: $B_{ab}=\frac{\mathcal{Z}_a}{\mathcal{Z}_b}$, or, equivalently, through the difference in logarithmic evidence $\Delta\ln\mathcal{Z}=\ln\mathcal{Z}_a-\ln\mathcal{Z}_b$. A higher value of $\ln\mathcal{Z}$ indicates stronger statistical support for the model, while a lower value suggests weaker support. The strength of evidence is interpreted using the revised Jeffreys scale (R. E. Kass & A. E. Raftery 1995):

1. $|\Delta\ln\mathcal{Z}|<1$, inconclusive/weak evidence,
2. $1\leqslant|\Delta\ln\mathcal{Z}|<3$, moderate evidence,
3. $3\leqslant|\Delta\ln\mathcal{Z}|<5$, strong evidence,
4. $|\Delta\ln\mathcal{Z}|\geqslant5$, decisive evidence.

In addition to the logarithmic Bayesian evidence, we compute the difference in the minimum chi-square, $\Delta\chi^2_{\rm min}$, defined as $\Delta\chi^2_{\rm min}\equiv\chi^2_{\rm min,\Lambda CDM}-\chi^2_{\rm min,Model}$. While $\Delta\chi^2_{\rm min}$ quantifies the improvement in the goodness of fit relative to the ΛCDM model, the Bayesian evidence provides a complementary criterion for the model comparison that naturally incorporates both the quality of the fit and the complexity of the model. Together, these two statistics offer a consistent and robust assessment of the preference for dynamical dark energy.

In our analysis, we adopt several assumptions. Specifically, for a dynamical dark-energy model, we assume a flat scenario ($\Omega_k=0$) and compute the present-day radiation density parameter as $\Omega_r=2.469\times10^{-5}h^{-2}(1+0.2271N_{\rm eff})$ following E. Komatsu et al. (2009), where $N_{\rm eff}=3.04$ is the standard effective number of relativistic species (G. Mangano et al. 2002). Under these assumptions, the dark-energy density parameter is given by $\Omega_\Lambda=1-\Omega_r-\Omega_m-\Omega_k$. In the case of the flat Universe $\Omega_k=0$, this realization reduces to $\Omega_\Lambda=1-\Omega_r-\Omega_m$. As a result, both Ω_Λ and Ω_r are not treated as independent parameters, since they are fully determined by the remaining parameters. The priors chosen for these models are summarized in Table 2.

4. Results

In cosmology, most anomalies such as the Hubble tension, the S_8 discrepancy, the M_B calibration offset, and the CMB lensing anomaly typically show deviations in the range of 2σ–4σ. While not definitive, such levels are considered statistically significant and often prompt further investigation. Here, we carry out such an analysis by exploring a range of cosmological models and their compatibility with current observational datasets. To quantitatively assess departures from the ΛCDM reference model, we introduce a dimensionless tension estimator, $T\equiv\frac{|x_{\rm model}-x_{\Lambda\rm CDM}|}{\sqrt{\sigma^2_{\rm model}+\sigma^2_{\Lambda\rm CDM}}}$, where $x_{\rm model}$ and $x_{\Lambda\rm CDM}$ denote the inferred values of a given cosmological parameter (such as h, Ω_m, ω_0, etc.) in the considered model and in ΛCDM, respectively, and $\sigma_{\rm model}$ and $\sigma_{\Lambda\rm CDM}$ represent their corresponding uncertainties. The magnitude of T is interpreted as follows: $T<1\sigma$ indicates consistency with ΛCDM; $1\sigma\leqslant T<2\sigma$ corresponds to a weak and statistically insignificant deviation; $2\sigma\leqslant T<3\sigma$ reflects mild tension; $3\sigma\leqslant T<5\sigma$ indicates moderate tension; and $T\geqslant5\sigma$ signifies a strong deviation.

Table 3 shows the numerical values of the corresponding parameters for the ΛCDM, oΛCDM, ωCDM, $\omega_0\omega_a$CDM,

Table 2
The Parameters and Their Priors including Uniform Priors $\mathcal{U}$ and the Reduced Hubble Constant $h \equiv H_0/100$

Model	Parameter	Prior
ΛCDM	Ω_{m0}	$\mathcal{U}[0, 1]$
	$h = H_0/100$	$\mathcal{U}[0, 1]$
oΛCDM	Ω_{k0}	$\mathcal{U}[-1, 1]$
	Ω_{m0}, h	$\mathcal{U}[0, 1]$
ωCDM	ω	$\mathcal{U}[-3, 1]$
	Ω_{m0}, h	$\mathcal{U}[0, 1]$
oωCDM	ω	$\mathcal{U}[-3, 1]$
	Ω_{k0}	$\mathcal{U}[-1, 1]$
	Ω_{m0}, h	$\mathcal{U}[0, 1]$
$\omega_0\omega_a$CDM	ω_0	$\mathcal{U}[-3, 1]$
	ω_a	$\mathcal{U}[-3, 2]$
	Ω_{m0}, h	$\mathcal{U}[0, 1]$
Logarithmic	ω_0	$\mathcal{U}[-3, 1]$
	ω_a	$\mathcal{U}[-3, 2]$
	Ω_{m0}, h	$\mathcal{U}[0, 1]$
Exponential	ω_0	$\mathcal{U}[-3, 1]$
	ω_a	$\mathcal{U}[-3, 2]$
	Ω_{m0}, h	$\mathcal{U}[0, 1]$
JBP	ω_0	$\mathcal{U}[-3, 1]$
	ω_a	$\mathcal{U}[-3, 2]$
	Ω_{m0}, h	$\mathcal{U}[0, 1]$
BA	ω_0	$\mathcal{U}[-3, 1]$
	ω_a	$\mathcal{U}[-3, 2]$
	Ω_{m0}, h	$\mathcal{U}[0, 1]$
GEDE	Δ	$\mathcal{U}[-10, 10]$
	Ω_{m0}, h	$\mathcal{U}[0, 1]$

logarithmic, exponential, JBP, BA, and GEDE models using MCMC analysis. Figure 1 shows the corner plots of each cosmological model using combinations of DESI DR2, different SNe Ia catalogs, and CC measurements. The diagonal panels show the 1D marginalized posterior distributions for each parameter, while the off-diagonal panels show the 2D marginalized confidence contours at 68% and 95% confidence levels (CLs).

First, we also obtain numerical values obtained from the CC measurements alone. For the ΛCDM model, we find $h = 0.662^{+0.053}_{-0.048}$ (hereafter referred to as the ΛCDM value), consistent with M. Moresco et al. (2012), M. Moresco (2015), and M. Moresco et al. (2016). Among its simple extensions, oΛCDM predicts $h = 0.674 \pm 0.053$, corresponding to a 0.16σ deviation from the ΛCDM value, while GEDE predicts $h = 0.678 \pm 0.053$, deviating by 0.21σ. ωCDM yields $h = 0.689^{+0.087}_{-0.097}$, showing a slight tension of 0.24σ relative to the value of ΛCDM. In contrast, the oωCDM model predicts $h = 0.716^{+0.077}_{-0.089}$, showing about a 0.52σ deviation from the ΛCDM value. Similarly, the $\omega_0\omega_a$CDM model yields $h = 0.727 \pm 0.082$, corresponding to a 0.67σ deviation, while the JBP model gives $h = 0.728^{+0.084}_{-0.072}$, with a deviation of 0.74σ. The BA parameterization predicts $h = 0.733 \pm 0.079$, marking the largest shift among these models at 0.75σ. Among other parameterizations, the logarithmic model estimates $h = 0.731 \pm 0.081$ (0.71σ deviation), and the exponential model provides the highest shift, $h = 0.736 \pm 0.079$, with a deviation of 0.78σ relative to the ΛCDM value, although tensions remain below 1σ, indicating consistency with ΛCDM.

We further analyzed the deviations of the Hubble parameter h and Ω_{m0} for each dark-energy model relative to the ΛCDM model, incorporating the CC dataset together with DESI DR2 and different SNe Ia catalogs. The combined CC + DESI DR2 dataset shows good agreement with the ΛCDM model across most dark-energy parameterizations. In particular, the oΛCDM, ωCDM, oωCDM, JBP, and GEDE models show deviations below the 1σ level in h (with $T_h = 0.64\sigma$, 0.48σ, 0.44σ, 0.91σ, and 0.40σ, respectively), indicating that the corresponding values of the Hubble parameter h remain fully consistent with the ΛCDM prediction. In contrast, the $\omega_0\omega_a$CDM, logarithmic, exponential, and BA parameterizations show weak and statistically insignificant tension in h, with deviations of 1.19σ, 1.38σ, 1.83σ, and 1.57σ, respectively.

For the matter density parameter Ω_{m0}, a very similar behavior is observed. The oΛCDM, ωCDM, oωCDM, JBP, and GEDE models show deviations below the 1σ level (with $T_{\Omega_m} = 0.28\sigma$, 0.08σ, 0.06σ, 0.86σ, and 0.08σ, respectively), indicating that the inferred values of Ω_{m0} remain fully consistent with the ΛCDM prediction. In contrast, the $\omega_0\omega_a$CDM, logarithmic, exponential, and BA parameterizations show weak and statistically insignificant tension in Ω_{m0}, with deviations of 1.11σ, 1.68σ, 1.67σ, and 1.62σ, respectively.

For the CC + DESI DR2 + Pantheon$^+$ dataset, the $\omega_0\omega_a$CDM, logarithmic, exponential, JBP, and BA models show deviations below the 1σ level in h (with $T_h = 0.56\sigma$, 0.56σ, 0.62σ, 0.86σ, and 0.50σ, respectively), indicating consistency with the ΛCDM model. In contrast, the oΛCDM, ωCDM, oωCDM, and GEDE models show weak and statistically insignificant tension in h, with deviations of 1.13σ, 1.22σ, 1.11σ, and 1.27σ, respectively. For the matter density parameter Ω_{m0}, the oΛCDM, ωCDM, oωCDM, $\omega_0\omega_a$CDM, logarithmic, exponential, JBP, BA, and GEDE models remain consistent with ΛCDM, with all lying below the 1σ level (with $T_{\Omega_m} = 0.83\sigma$, 0.53σ, 0.22σ, 0.13σ, 0.13σ, 0.07σ, 0.12σ, 0.26σ, and 0.53σ, respectively).

For the CC + DESI DR2 + DES-Dovekie dataset, the oΛCDM, $\omega_0\omega_a$CDM, logarithmic, exponential, JBP, and BA models show deviations below the 1σ level in h (with $T_h = 0.90\sigma$, 0.32σ, 0.28σ, 0.30σ, 0.51σ, and 0.29σ, respectively), indicating consistency with the ΛCDM model. In contrast, the ωCDM, oωCDM, and GEDE models show weak and statistically insignificant tension in h, with deviations of 1.38σ, 1.48σ, and 1.33σ, respectively. For the matter density parameter Ω_{m0}, the oΛCDM, ωCDM, oωCDM, $\omega_0\omega_a$CDM, logarithmic, exponential, JBP, BA, and GEDE models remain consistent with ΛCDM, with all deviations lying below the 1σ level (with $T_{\Omega_m} = 0.79\sigma$, 0.61σ, 0.58σ, 0.68σ, 0.84σ, 0.79σ, 0.50σ, 0.72σ, and 0.56σ, respectively).

Finally, for the CC + DESI DR2 + Union3 dataset, the $\omega_0\omega_a$CDM, logarithmic, exponential, and BA models show deviations of 0.95σ, 0.92σ, 0.99σ, and 0.91σ in h, respectively, indicating consistency with ΛCDM. In contrast, the oΛCDM, ωCDM, oωCDM, JBP, and GEDE models show weak and statistically insignificant tension in h, with deviations of 1.06σ, 1.78σ, 1.41σ, 1.42σ, and 1.18σ, respectively. For the matter density parameter Ω_{m0}, the oΛCDM, ωCDM, oωCDM, and

Table 3

The Numerical Constraints on the oΛCDM, ωCDM, oωCDM, $\omega_0\omega_a$CDM, Logarithmic, Exponential, JBP, BA, and GEDE Models at the 68% (1σ) Confidence Level, Obtained Using Combinations of DESI DR2 with CC Measurements and Different SNe Ia Catalogs (Pantheon$^+$, DES-Dovekie, and Union3)

Dataset/Models	h	Ω_m	Ω_k	ω or ω_0	ω_a	Δ	$\lvert\Delta \ln \mathcal{Z}_{\Lambda\mathrm{CDM,Model}}\rvert$	$\Delta\chi^2_{\mathrm{min}}$
ΛCDM								
CC + DESI DR2	0.692 ± 0.010	0.297 ± 0.008	⋯	⋯	⋯	⋯	0	0
CC + DESI DR2 + Pantheon$^+$	0.691 ± 0.010	0.304 ± 0.008	⋯	⋯	⋯	⋯	0	0
CC + DESI DR2 + DES-Dovekie	0.691 ± 0.010	0.305 ± 0.007	⋯	⋯	⋯	⋯	0	0
CC + DESI DR2 + Union3	0.691 ± 0.010	0.303 ± 0.008	⋯	⋯	⋯	⋯	0	0
oΛCDM								
CC + DESI DR2	0.683 ± 0.010	0.293 ± 0.012	0.027 ± 0.041	⋯	⋯	⋯	2.14	0.18
CC + DESI DR2 + Pantheon$^+$	0.675 ± 0.010	0.292 ± 0.012	0.051 ± 0.036	⋯	⋯	⋯	1.53	0.88
CC + DESI DR2 + DES-Dovekie	0.674 ± 0.016	0.294 ± 0.012	0.053 ± 0.037	⋯	⋯	⋯	1.36	1.04
CC + DESI DR2 + Union3	0.676 ± 0.010	0.294 ± 0.011	0.050 ± 0.039	⋯	⋯	⋯	1.51	0.86
ωCDM								
CC + DESI DR2	0.675 ± 0.034	0.296 ± 0.009	⋯	$-0.951^{+0.110}_{-0.091}$	⋯	⋯	1.17	0.20
CC + DESI DR2 + Pantheon$^+$	0.667 ± 0.017	0.298 ± 0.008	⋯	-0.923 ± 0.044	⋯	⋯	0.47	1.74
CC + DESI DR2 + DES-Dovekie	0.665 ± 0.016	0.298 ± 0.009	⋯	-0.917 ± 0.039	⋯	⋯	0.02	2.28
CC + DESI DR2 + Union3	0.648 ± 0.022	0.298 ± 0.009	⋯	-0.867 ± 0.058	⋯	⋯	0.96	2.87
oωCDM								
CC + DESI DR2	$0.677^{+0.033}_{-0.040}$	$0.296^{+0.014}_{-0.011}$	$0.049^{+0.066}_{-0.078}$	$-1.09^{+0.28}_{-0.13}$	⋯	⋯	2.70	0.19
CC + DESI DR2 + Pantheon$^+$	0.660 ± 0.026	0.301 ± 0.011	$0.019^{+0.049}_{-0.056}$	$-0.937^{+0.064}_{-0.056}$	⋯	⋯	2.48	1.73
CC + DESI DR2 + DES-Dovekie	0.663 ± 0.016	0.297 ± 0.012	0.002 ± 0.049	$-0.918^{+0.055}_{-0.046}$	⋯	⋯	2.18	2.28
CC + DESI DR2 + Union3	0.649 ± 0.028	0.298 ± 0.012	$-0.002^{+0.045}_{-0.058}$	$-0.865^{+0.076}_{-0.062}$	⋯	⋯	1.05	2.92
$\omega_0\omega_a$CDM								
CC + DESI DR2	$0.652^{+0.032}_{-0.041}$	$0.337^{+0.048}_{-0.035}$	⋯	$-0.61^{+0.37}_{-0.32}$	$-1.20^{+1.0}_{-1.3}$	⋯	0.94	1.44
CC + DESI DR2 + Pantheon$^+$	$0.676^{+0.025}_{-0.021}$	$0.306^{+0.020}_{-0.013}$	⋯	$-0.889^{+0.059}_{-0.068}$	$-0.31^{+0.51}_{-0.43}$	⋯	0.25	1.85
CC + DESI DR2 + DES-Dovekie	$0.683^{+0.023}_{-0.019}$	$0.315^{+0.017}_{-0.013}$	⋯	$-0.838^{+0.068}_{-0.086}$	$-0.65^{+0.59}_{-0.48}$	⋯	0.93	3.02
CC + DESI DR2 + Union3	0.668 ± 0.022	$0.330^{+0.019}_{-0.014}$	⋯	-0.70 ± 0.11	-1.07 ± 0.58	⋯	3.02	4.88
Logarithmic								
CC + DESI DR2	$0.647^{+0.031}_{-0.038}$	$0.354^{+0.042}_{-0.033}$	⋯	-0.52 ± 0.29	$-1.29^{+0.78}_{-0.88}$	⋯	0.96	1.47
CC + DESI DR2 + Pantheon$^+$	$0.676^{+0.025}_{-0.022}$	$0.306^{+0.020}_{-0.013}$	⋯	$-0.893^{+0.052}_{-0.059}$	$-0.27^{+0.39}_{-0.31}$	⋯	1.03	1.92
CC + DESI DR2 + DES-Dovekie	$0.684^{+0.023}_{-0.018}$	$0.316^{+0.018}_{-0.011}$	⋯	$-0.855^{+0.056}_{-0.064}$	-0.50 ± 0.40	⋯	0.63	3.03
CC + DESI DR2 + Union3	0.668 ± 0.023	$0.331^{+0.020}_{-0.015}$	⋯	$-0.729^{+0.091}_{-0.11}$	$-0.80^{+0.48}_{-0.43}$	⋯	2.92	4.57
Exponential								
CC + DESI DR2	$0.629^{+0.033}_{-0.041}$	0.375 ± 0.046	⋯	-0.77 ± 0.14	-1.07 ± 0.63	⋯	0.51	1.46
CC + DESI DR2 + Pantheon$^+$	$0.675^{+0.024}_{-0.020}$	$0.305^{+0.017}_{-0.012}$	⋯	-0.955 ± 0.061	$-0.13^{+0.20}_{-0.18}$	⋯	1.03	1.85
CC + DESI DR2 + DES-Dovekie	$0.684^{+0.021}_{-0.019}$	$0.316^{+0.016}_{-0.012}$	⋯	-0.978 ± 0.058	$-0.30^{+0.24}_{-0.21}$	⋯	0.13	3.04
CC + DESI DR2 + Union3	0.668 ± 0.021	$0.331^{+0.018}_{-0.015}$	⋯	-0.938 ± 0.063	$-0.51^{+0.29}_{-0.26}$	⋯	1.85	4.52
JBP								
CC + DESI DR2	$0.659^{+0.035}_{-0.040}$	$0.314^{+0.025}_{-0.018}$	⋯	$-0.72^{+0.33}_{-0.20}$	$-1.66^{+0.74}_{-1.6}$	⋯	0.77	1.11
CC + DESI DR2 + Pantheon$^+$	0.671 ± 0.021	$0.302^{+0.014}_{-0.012}$	⋯	-0.888 ± 0.087	$-0.36^{+0.78}_{-0.69}$	⋯	0.18	1.78
CC + DESI DR2 + DES-Dovekie	0.680 ± 0.019	$0.312^{+0.014}_{-0.012}$	⋯	-0.799 ± 0.098	-1.08 ± 0.80	⋯	1.51	3.07
CC + DESI DR2 + Union3	0.658 ± 0.021	$0.320^{+0.015}_{-0.013}$	⋯	$-0.66^{+0.14}_{-0.11}$	$-1.56^{+0.63}_{-1.0}$	⋯	3.41	4.50

Table 3
(Continued)

Dataset/Models	h	Ω_m	Ω_k	ω or ω_0	ω_a	Δ	$\lvert\Delta \ln \mathcal{Z}_{\Lambda\mathrm{CDM,Model}}\rvert$	$\Delta\chi^2_{\mathrm{min}}$
BA								
CC + DESI DR2	$0.638^{+0.033}_{-0.040}$	0.363 ± 0.040	⋯	$-0.46^{+0.29}_{-0.34}$	$-0.99^{+0.64}_{-0.54}$	⋯	0.54	1.49
CC + DESI DR2 + Pantheon$^+$	$0.678^{+0.024}_{-0.021}$	$0.308^{+0.017}_{-0.013}$	⋯	-0.898 ± 0.056	$-0.19^{+0.26}_{-0.21}$	⋯	0.70	1.94
CC + DESI DR2 + DES-Dovekie	$0.684^{+0.022}_{-0.019}$	$0.315^{+0.016}_{-0.012}$	⋯	$-0.865^{+0.050}_{-0.061}$	$-0.32^{+0.27}_{-0.22}$	⋯	0.16	2.98
CC + DESI DR2 + Union3	0.669 ± 0.022	$0.330^{+0.018}_{-0.015}$	⋯	-0.740 ± 0.095	$-0.54^{+0.32}_{-0.28}$	⋯	2.62	4.53
GEDE								
CC + DESI DR2	0.677 ± 0.036	0.298 ± 0.009	⋯	⋯	⋯	$-0.20^{+0.60}_{-0.86}$	0.70	0.21
CC + DESI DR2 + Pantheon$^+$	0.667 ± 0.016	0.298 ± 0.008	⋯	⋯	⋯	$-0.46^{+0.24}_{-0.27}$	1.28	1.76
CC + DESI DR2 + DES-Dovekie	0.667 ± 0.015	0.299 ± 0.008	⋯	⋯	⋯	$-0.50^{+0.20}_{-0.25}$	1.83	2.34
CC + DESI DR2 + Union3	0.647 ± 0.036	0.300 ± 0.008	⋯	⋯	⋯	$-0.84^{+0.28}_{-0.34}$	2.80	3.05

Note. The bold values in Table 3 highlight the individual model results.

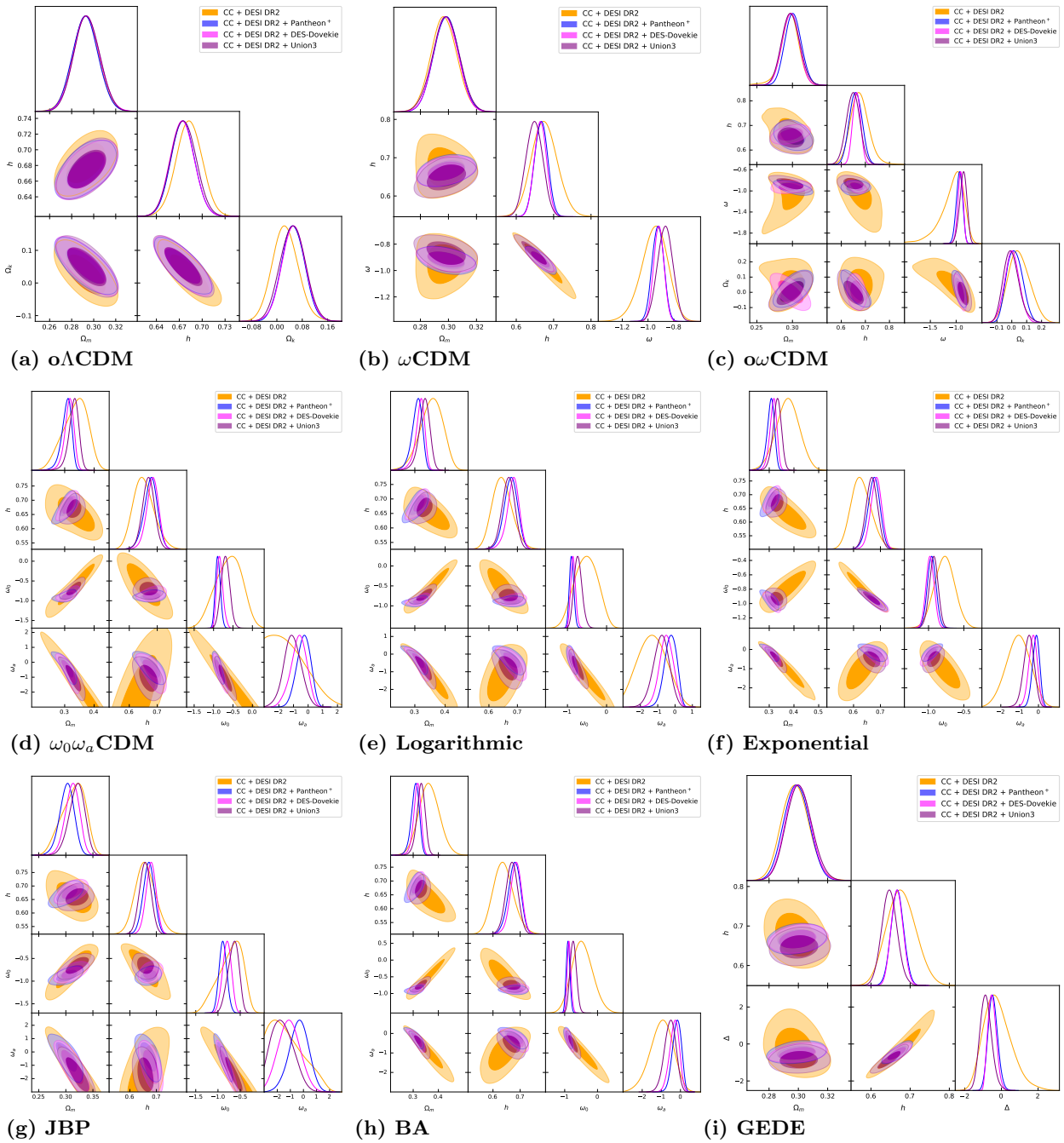

Figure 1. This figure shows the corner plots for the (a) oΛCDM, (b) ωCDM, (c) oωCDM, (d) $\omega_0\omega_a$CDM, (e) logarithmic, (f) exponential, (g) JBP, (h) BA, and (i) GEDE models, obtained using DESI DR2 with CC measurements and different SNe Ia catalogs (Pantheon$^+$, DES-Dovekie, and Union3), at the 68% (1σ) and 95% (2σ) confidence levels.

GEDE models remain consistent with ΛCDM, with deviations of 0.66σ, 0.42σ, 0.35σ, and 0.27σ, respectively. In contrast, the $\omega_0\omega_a$CDM, logarithmic, exponential, JBP, and BA parameterizations show weak and statistically insignificant tension in Ω_{m0}, with deviations of 1.67σ, 1.65σ, 1.65σ, 1.11σ, and 1.59σ, respectively.

Figure 2 shows the different parameter planes of various cosmological models. These planes provide insights into the geometry of the Universe and the nature of dark energy. Panels (a), (b), and (c) of Figure 2 show the $\omega-\Omega_m$, $\omega-\Omega_k$, and $\Omega_m-\Omega_k$ planes for the oΛCDM, ωCDM, and oωCDM models, respectively. It is important to note that, in the case of the oΛCDM model, for all combinations of the datasets, the inferred curvature parameter is greater than zero, indicating a preference for an open Universe, which is compatible with recent late-time observations supporting an open Universe (P.-J. Wu & X. Zhang 2025). A similar behavior is observed in the oωCDM model for the CC + DESI DR2 and CC + DESI DR2 + Pantheon$^+$ combinations. While in the oωCDM model, when the DES-Dovekie and Union3 datasets are included, the corresponding values are consistent with a spatially flat Universe, in agreement with the Wilkinson Microwave Anisotropy Probe (WMAP; $-0.0179 < \Omega_k < 0.0081$, 95% CL; G. Hinshaw et al. 2009), BOOMERanG ($0.88 < \Omega_{M/R}$

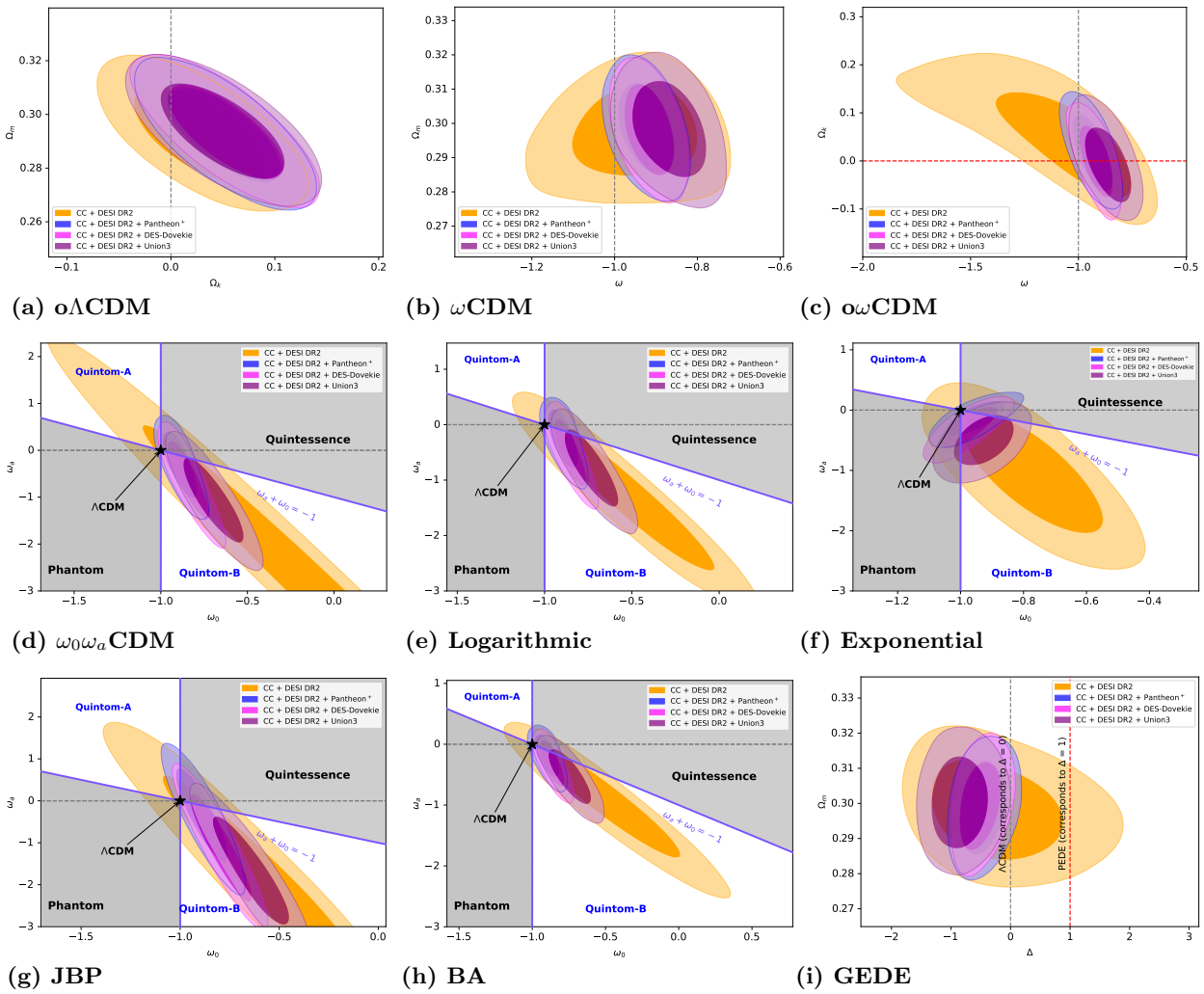

Figure 2. This figure shows the posterior distributions of different planes of the (a) oΛCDM, (b) ωCDM, (c) oωCDM, (d) $\omega_0\omega_a$CDM, (e) logarithmic, (f) exponential, (g) JBP, (h) BA, and (i) GEDE models, obtained using DESI DR2 with CC measurements and different SNe Ia catalogs (Pantheon$^+$, DES-Dovekie, and Union3), at the 68% (1σ) and 95% (2σ) confidence levels.

$+ \Omega_\Lambda < 1.0081$, 95% CL; P. De Bernardis et al. 2000), and Planck ($\Omega_{M/R} + \Omega_\Lambda = 1.00 \pm 0.026$, 68% CL; N. Aghanim et al. 2020).

We also observe that, in the cases of the ωCDM and oωCDM models, the predicted value of ω in each case, $\omega_0 > -1$, shows a deviation from $\omega = -1$. However, in the oωCDM model, when we consider the combination CC + DESI DR2, we obtain $\omega_0 \approx -1$, which is close to the ΛCDM prediction. We also observe that in both cases the inclusion of different SNe Ia catalogs (Pantheon$^+$, DES-Dovekie, and Union3) shows a larger deviation from $\omega = -1$ compared to the CC + DESI DR2 combination alone.

Panels (d)–(h) of Figure 2 show the $\omega_0 - \omega_a$ planes for the $\omega_0\omega_a$CDM, logarithmic, exponential, JBP, and BA models, respectively. These provide important insights into the nature of dark energy. Each model predicts the values in the $\omega_0 > -1$ and $\omega_a < 0$ quadrant for each combination of DESI DR2 datasets with CC and different SNe Ia calibrations, showing the preference for dark energy characterized by $\omega_0 > -1$, $\omega_a < 0$, and $\omega_0 + \omega_a < -1$, corresponding to a Quintom-B type behavior (Y. Cai et al. 2025; G. Ye et al. 2025), where the dark-energy EoS parameter transitions from $\omega < -1$ in the past to $\omega > -1$ at the present epoch.

On the other hand, panel (i) of Figure 2 shows the Δ–Ω_m plane for the GEDE model, where the parameter Δ describes the evolution slope of the dark-energy density, and the parameter z_t denotes the transition redshift at which the dark-energy density becomes equal to the matter density. Indeed, z_t is not a free parameter but is determined by the condition that the dark-energy density equals the matter density (X. Li & A. Shafieloo 2020). The GEDE model reduces to the ΛCDM model for $\Delta = 0$ and to the phenomenologically emergent dark-energy model (X. Li & A. Shafieloo 2019) for $\Delta = 1$. It is crucial to note that, in each case, the GEDE model predicts a negative value of Δ, indicating an injection of dark energy at high redshifts. Indeed, these results deviate from those reported by K. Lodha et al. (2025b, 2025a), H. Chaudhary et al. (2025b, 2026), since they consider the CMB in their analysis. Thus, one can also see the effect of late-time measurements on the predicted value of Δ.

Figure 3 shows the preference for dynamical dark energy over the cosmological constant (Λ), quantified in terms of the statistical significance departure from $\omega_0 = -1$. It can be observed that, for the DESI DR2 + CC dataset, the ωCDM and oωCDM models show deviations below 1σ, while the

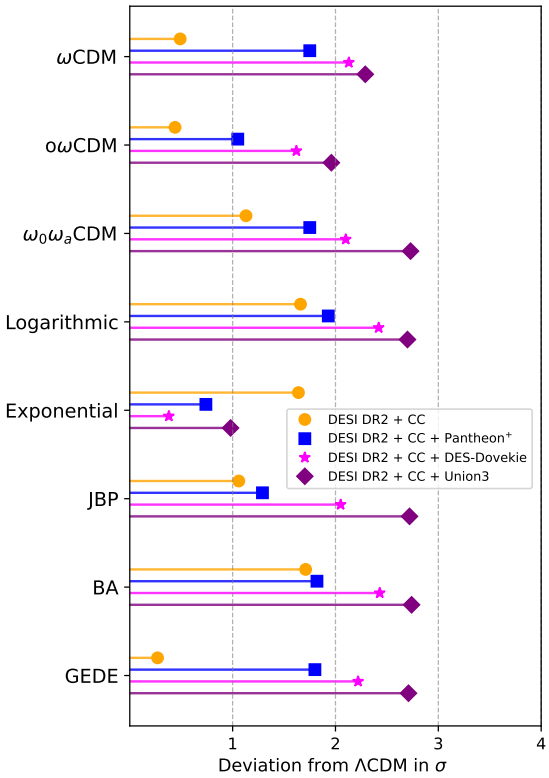

Figure 3. This figure shows the statistical deviation (in units of σ) of each dark-energy model relative to the ΛCDM model, defined by $\omega = -1$ (and $\Delta = 0$ for the GEDE model). These results are obtained using DESI DR2 with CC measurements and different SNe Ia catalogs (Pantheon$^+$, DES-Dovekie, and Union3).

$\omega_0\omega_a$CDM, logarithmic, exponential, JBP, and BA models show deviations of about 1.13σ, 1.66σ, 1.64σ, 1.06σ, and 1.71σ, respectively. Indeed, all these deviations remain below the 2σ level, indicating the weak preference of dynamical dark energy. For the DESI DR2 + CC + Pantheon$^+$ dataset, the preference for dynamical dark energy increases noticeably for most models. The ωCDM and $\omega_0\omega_a$CDM models both show deviations of about 1.75σ, while the oωCDM model shows a deviation of 1.05σ. The logarithmic, JBP, and BA models show deviations at the level of 1.93σ, 1.29σ, and 1.82σ, respectively, whereas the exponential model shows the weakest deviation, remaining below 1σ at 0.74σ.

For the DESI DR2 + CC + DES-Dovekie dataset, the preference for dynamical dark energy increases for most models. The ωCDM, $\omega_0\omega_a$CDM, logarithmic, JBP, and BA models show deviations of about 2.13σ, 2.10σ, 2.42σ, 2.05σ, and 2.43σ, respectively, while the oωCDM model shows the smaller deviation of 1.62σ. In contrast, the exponential model shows a weaker preference for dynamical dark energy, remaining below 1σ at about 0.38σ. For the DESI DR2 + CC + Union3 dataset, the ωCDM, $\omega_0\omega_a$CDM, logarithmic, JBP, and BA models show deviations of about 2.29σ, 2.73σ, 2.70σ, 2.72σ, and 2.74σ, respectively, while the oωCDM model shows a preference of 1.96σ. Once again, the exponential model shows the weakest deviation, remaining below 1σ at 0.98σ.

Finally, for the GEDE model, the preference for dynamical dark energy can be quantified by estimating the deviation from $\Delta = 0$. For the DESI DR2 + CC dataset, it shows a deviation of 0.27σ. With the inclusion of the Pantheon$^+$ data, the GEDE model shows a deviation of about 1.80σ, and for the DESI DR2 + CC + DES-Dovekie dataset, it shows a deviation of about 2.22σ. For the DESI DR2 + CC + Union3 dataset, the deviation further increases and reaches 2.71σ. Indeed, none of the cases reaches the 3σ level of deviation in the preference for dynamical dark energy. Although the DESI DR2 data show hints of new physics, the ΛCDM model remains consistent with the observations and is not yet ruled out by the late-time measurements.

Figure 4 shows the comparative analysis of each dark-energy model relative to the ΛCDM model based on the logarithmic Bayesian evidence, using the revised Jeffreys' scale. For the CC + DESI DR2 dataset, the oΛCDM, ωCDM, and oωCDM models show moderate evidence, while all other models show weak evidence. For the CC + DESI DR2 + Pantheon$^+$ combination, the oΛCDM, oωCDM, logarithmic, exponential, and GEDE models show moderate evidence, whereas the remaining models show weak evidence. For the CC + DESI DR2 + DES-Dovekie combination, the oΛCDM, oωCDM, JBP, and GEDE models show moderate evidence, while all other models remain weak evidence. Finally, for the CC + DESI DR2 + Union3 combination, the oΛCDM, oωCDM, exponential, BA, and GEDE models show moderate evidence, while the ωCDM model shows weak evidence, and the $\omega_0\omega_a$CDM and JBP models show strong evidence. The corresponding numerical values associated with the logarithmic Bayesian evidence can be seen in the eighth column of Table 3.

A complementary perspective is provided by the best-fit goodness-of-fit improvements, quantified by $\Delta\chi^2_{\rm min}$. For CC + DESI DR2, all models show only marginal improvement with $\Delta\chi^2_{\rm min} \lesssim 1.5$, indicating no strong deviation from ΛCDM, while the inclusion of Pantheon$^+$ slightly strengthens the preference for dynamical models, with $\Delta\chi^2_{\rm min} \approx 1.7$–$1.9$. The DES-Dovekie combination yields more pronounced improvements, with several models reaching $\Delta\chi^2_{\rm min} \approx 3$, including $\omega_0\omega_a$CDM, logarithmic, exponential, JBP, and BA. The strongest gains arise for the Union3 dataset, most notably for $\omega_0\omega_a$CDM ($\Delta\chi^2_{\rm min} = 4.88$), followed by logarithmic, exponential, BA, and JBP. These $\Delta\chi^2_{\rm min}$ improvements are consistent with the Bayesian evidence results and further support the conclusion that Union3 provides the most compelling indication of departures from ΛCDM.

Figure 5 shows the redshift evolution of the EoS parameter $\omega(z)$ for each dark-energy parameterization, using different combinations of datasets (DESI DR2, CC, Pantheon$^+$, DES-Dovekie, and Union3). In each model, with some exceptions for each combination of dataset, it can be observed that $\omega(z)$ falls below $\omega = -1$ at redshifts $z \gtrsim 0.5$, indicating a phantom regime ($\omega < -1$). At lower redshifts, around $z \lesssim 0.5$, $\omega(z)$ rises back above -1, entering the quintessence-like regime ($\omega > -1$). This crossing, where $\omega(z)$ evolves from the phantom to the quintessence regime by crossing $\omega = -1$, is known as phantom crossing, and this behavior, where the models show phantom behavior in the past and quintessence behavior in the present, is characterized by the quintom-B type scenario (Y. Cai et al. 2025; G. Ye et al. 2025). The first exception is the $\omega_0\omega_a$CDM model with the DESI DR2 + CC + Pantheon$^+$ combination, where the phantom crossing occurs around $z \approx 0.6$, while for the JBP model with the DESI DR2 + CC combination it occurs around $z \approx 0.65$. There is another expectation that, for each data combination, the mean value of

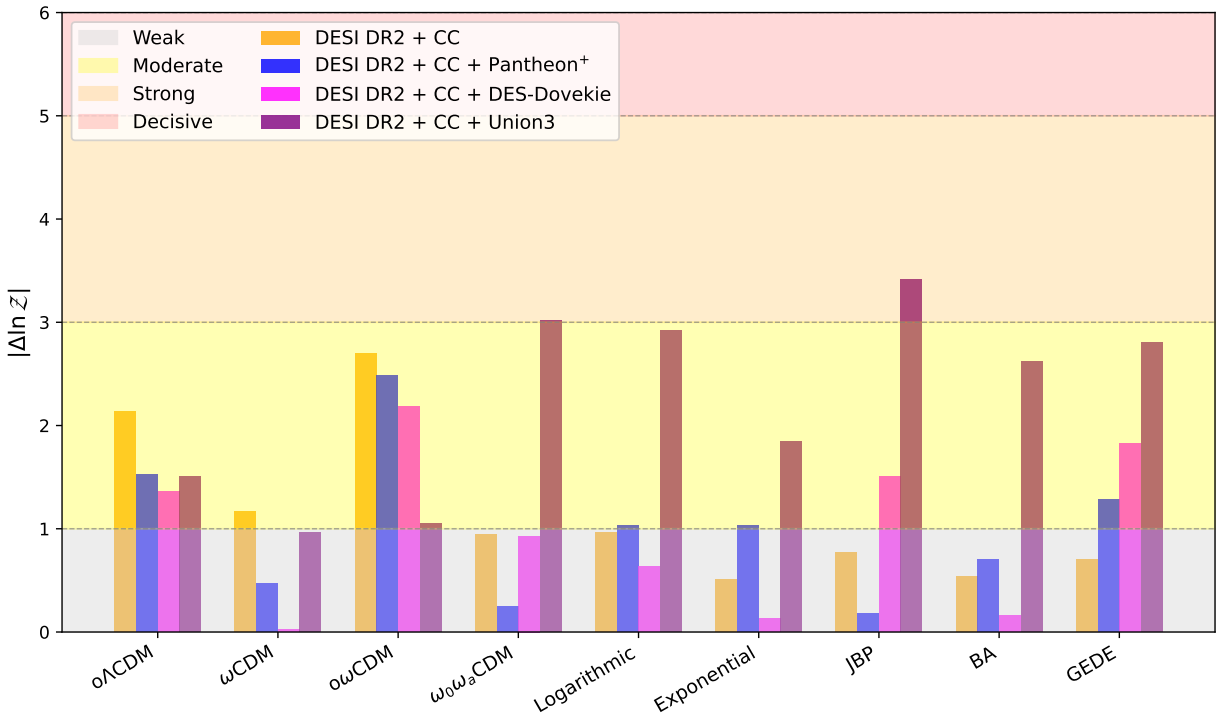

Figure 4. This figure shows the difference in logarithmic Bayesian evidence of each dark-energy model relative to the ΛCDM model using DESI DR2 with CC measurements and different SNe Ia catalogs (Pantheon$^+$, DES-Dovekie, and Union3).

$\omega(z)$ lies above $\omega = -1$ for the GEDE model and for the JBP model when combined with DESI DR2 + CC + Pantheon$^+$.

Figure 6 shows the redshift evolution of the energy density $f_{\rm DE}(z)$ presented in the third column of Table 2 for each dark-energy parameterization. It can be observed that, for all models, $f_{\rm DE}(z)$ converges to 1 at $z = 0$, i.e., $f_{\rm DE}(0) = 1$, for each combination of datasets. Also, for the GEDE model for each data combination and the JBP model with the DESI DR2 + CC, DESI DR2 + CC + Pantheon$^+$, and DESI DR2 + CC + Union3 combinations, the mean value of $f_{\rm DE}$ lies above $f_{\rm DE} = 1$, while all models cross $f_{\rm DE} = 1$ at different redshifts depending on the chosen datasets. In Figures 5 and 6, the solid lines represent the mean values, while the light shaded and dark shaded regions correspond to the 1σ and 2σ confidence intervals, respectively.

5. Discussion and Conclusions

In this work, we have carried out a comprehensive Bayesian MCMC analysis of several cosmological models including ΛCDM, oΛCDM, ωCDM, $\omega_0\omega_a$CDM, logarithmic, exponential, JBP, BA, and GEDE using the most recent BAO measurements from more than 14 million galaxies and QSO drawn from the DESI DR2 in combination with CC and different SNe Ia catalogs (Pantheon$^+$, DES-Dovekie, and Union3). We constrain the key cosmological parameters (h, Ω_m, Ω_k, ω_0, ω_a, and Δ) to investigate the preference for dynamical dark energy over the cosmological constant Λ.

Our results show that, using CC measurements alone, the ΛCDM model yields a reference value $h = 0.662^{+0.053}_{-0.048}$, while all dark-energy models predict slightly higher values of h, with deviations remaining below the 1σ level. This indicates that CC measurements alone do not provide statistically significant evidence for departures from ΛCDM. When CC data are combined with DESI DR2, the constraints on h and Ω_{m0} remain consistent with ΛCDM across most dark-energy parameterizations. The oΛCDM, ωCDM, oωCDM, JBP, and GEDE models show deviations below the 1σ level in both parameters, while the $\omega_0\omega_a$CDM, logarithmic, exponential, and BA models show comparatively larger but statistically insignificant deviations, not exceeding the $\sim 2\sigma$ level. The inclusion of SN Ia data (Pantheon$^+$, DES-Dovekie, and Union3) further improves the constraints without qualitatively altering these conclusions. In all cases, Ω_{m0} remains fully consistent with ΛCDM at the 1σ level, while mild, dataset-dependent deviations in h at the $\sim 1\sigma$–2σ level are observed for some models, remaining statistically insignificant.

Our results show that the oΛCDM model favors an open Universe for all combinations of the datasets. In contrast, for the oωCDM model, the CC + DESI DR2 and CC + DESI DR2 + Pantheon$^+$ combinations again favor an open Universe, while the CC + DESI DR2 + DES-Dovekie and CC + DESI DR2 + Union3 datasets favor a nearly flat Universe, supporting a spatially flat geometry consistent with WMAP, BOOMERanG, and Planck observations. Furthermore, the joint posterior analyses of the (ω_0, ω_a) parameter planes reveal that most dynamical dark-energy parameterizations favor $\omega_0 > -1$ and $\omega_a < 0$, indicating that such dynamical dark energy is characterized by a Quintom-B-type behavior.

Consequently, our analysis shows that, using late-time observations, dark-energy extensions beyond the cosmological constant exhibit deviations from ΛCDM below the 1σ level for the ωCDM, oωCDM, and GEDE models when the DESI DR2 + CC dataset is used, while the remaining dark-energy models show deviations that remain below the 2σ level. In contrast, when the Pantheon$^+$ SNe Ia dataset is included, most dynamical dark-energy models exhibit deviations from ΛCDM at the 1σ–2σ level when combined with DESI DR2 + CC data, while the oωCDM and exponential models remain below the

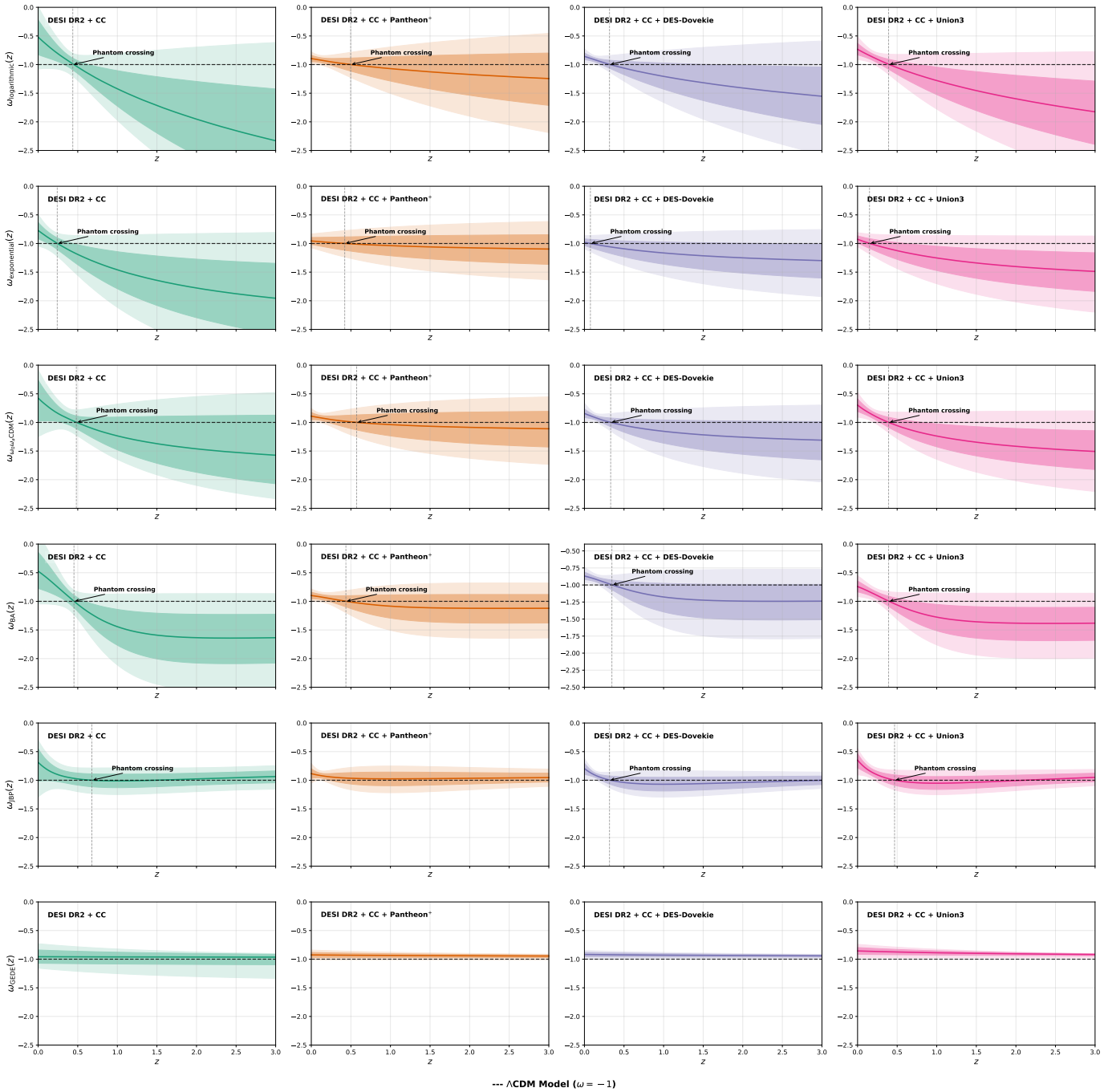

Figure 5. This figure shows the evolution of $\omega(z)$ as a function of redshift, using DESI DR2 with CC measurements and different SNe Ia catalogs (Pantheon$^+$, DES-Dovekie, and Union3).

1σ level. With the inclusion of the DES-Dovekie and Union3 SNe Ia datasets, most dynamical dark-energy models show deviations from ΛCDM at the 2σ–3σ level when combined with DESI DR2 + CC data, while the oωCDM model remains below the 2σ level, and the exponential model consistently shows deviations below 1σ. Indeed, these deviations show that the preference for dynamically dark energy reaches the 2σ–3σ level; yet, it remains insufficient to conclusively rule out the ΛCDM model.

Bayesian evidence and goodness-of-fit analyses show that the level of support for dark-energy extensions beyond ΛCDM depends strongly on the chosen dataset. While the CC + DESI DR2 combination provides at most moderate support for oΛCDM and oωCDM, with only small improvements in the fit ($\Delta\chi^2_{\rm min} \lesssim 1.5$), the inclusion of the Pantheon$^+$ sample slightly increases this preference ($\Delta\chi^2_{\rm min} \simeq 1.7$–$1.9$). In contrast, the DES-SN5Y and Union3 datasets give the strongest support for dynamical dark-energy models, such as $\omega_0\omega_a$CDM, JBP, BA, and GEDE, and show larger improvements in the fit, including the highest $\Delta\chi^2_{\rm min}$ values.

The evolution of the EoS parameter $\omega(z)$ shows that most dark-energy parameterizations undergo a transition from a phantom regime ($\omega < -1$) at intermediate redshifts to a quintessence-like regime ($\omega > -1$) at low redshifts, consistent

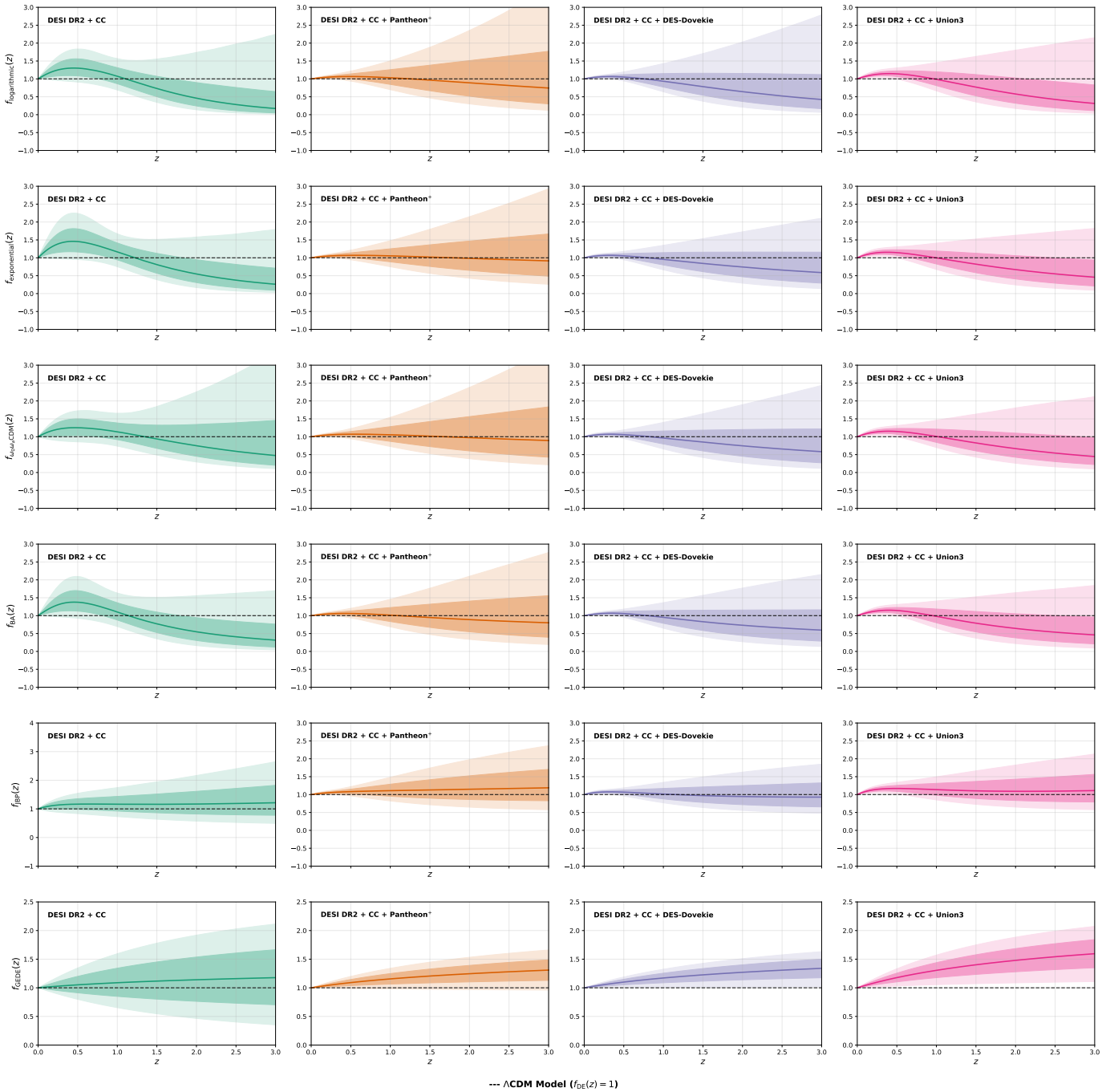

Figure 6. This figure shows the evolution of the energy density $f_{\rm DE}(z)$ as a function of redshift, using DESI DR2 with CC measurements and different SNe Ia catalogs (Pantheon^{+}, DES-Dovekie, and Union3).

with a phantom-crossing, quintom-B type behavior, with the transition redshift depending on the model and dataset. Notable exceptions include the GEDE model and the JBP model when combined with DESI DR2 + CC + Pantheon^{+}, for which the mean value of $\omega(z)$ remains above -1. The corresponding evolution of the normalized dark-energy density $f_{\rm DE}(z)$ satisfies $f_{\rm DE}(0) = 1$ for all cases and exhibits dataset-dependent crossings of $f_{\rm DE} = 1$, supporting a time-varying dark-energy component compatible with current observational constraints.

In conclusion, our analysis indicates that the standard ΛCDM cosmology remains a statistically robust description of the current Universe, although late-time observational datasets, particularly DESI DR2 and recent SNe Ia samples, provide moderate evidence supporting the possibility of dynamical dark-energy models. Future Stage IV surveys and next generation observatories are poised to significantly advance our understanding of the dark sector. DESI will deliver refined constraints from DR2 probes such as full-shape fitting, bispectrum, gravitational lensing, and peculiar velocities in 2025–2026, with DR3 results expected in 2027, which may shed light on the possible phantom crossing (P. Ade et al. 2019; K. Dawson et al. 2022) and the extent of any deviations from the ΛCDM model. The Nancy Grace Roman Space Telescope, launching in 2026, and the proposed DESI-II in the 2030s will probe the $z > 1$ Universe, opening a new frontier

for dark-energy studies (D. Spergel et al. 2015; K. Dawson et al. 2022). If Stage IV surveys break the ΛCDM model, developing new observational methods, cross-survey analyses, and searches for specific model signatures will be crucial, and a dedicated post-ΛCDM dark-energy task force could provide guidance for exploring the complex physics of the dark sector.

Acknowledgments

S.C. acknowledges the Istituto Nazionale di Fisica Nucleare (INFN) Sez. di Napoli, Iniziative Specifiche QGSKY and MoonLight-2 and the Istituto Nazionale di Alta Matematica (INdAM), gruppo GNFM, for the support. This paper is based upon work from COST Action CA21136—Addressing observational tensions in cosmology with systematics and fundamental physics (CosmoVerse), supported by COST (European Cooperation in Science and Technology). V.K.S. gratefully acknowledges the facilities and institutional support provided by the Indian Institute of Astrophysics (IIA), India, during his tenure as a postdoctoral fellow.

ORCID iDs

Himanshu Chaudhary https://orcid.org/0000-0002-6376-0707
Vipin Kumar Sharma https://orcid.org/0000-0001-7640-5504
Salvatore Capozziello https://orcid.org/0000-0003-4886-2024
G. Mustafa https://orcid.org/0000-0003-1409-2009

References

Abbott, T. M. C., Acevedo, M., Aguena, M., et al. 2024, ApJL, 973, L14
Abbott, T. M. C., Abdalla, F. B., Alarcon, A., et al. 2018, PhRvD, 98, 043526
Adame, A., Aguilar, J., Ahlen, S., et al. 2025, JCAP, 2025, 021
Ade, P., Aguirre, J., Ahmed, Z., et al. 2019, JCAP, 2019, 056
Ade, P. A. R., Aghanim, N., Armitage-Caplan, C., et al. 2014, A&A, 571, A16
Ade, P. A. R., Aghanim, N., Arnaud, M., et al. 2016, A&A, 594, A13
Aghanim, N., Akrami, Y., Ashdown, M., et al. 2020, A&A, 641, A6
Barboza, E., & Alcaniz, J. 2008, PhLB, 666, 415
Barua, S., & Desai, S. 2025, PDU, 49, 101995
Basilakos, S., & Nesseris, S. 2017, PhRvD, 96, 063517
Benetti, M., & Capozziello, S. 2019, JCAP, 12, 008
Betoule, M., Kessler, R., Guy, J., et al. 2014, A&A, 568, A22
Brout, D., Scolnic, D., Popovic, B., et al. 2022, ApJ, 938, 110
Cai, Y., Ren, X., Qiu, T., Li, M., & Zhang, X. 2025, arXiv:2505.24732
Capozziello, S., Chaudhary, H., Harko, T., & Mustafa, G. 2026, PDU, 51, 102196
Capozziello, S., & De Laurentis, M. 2011, PhR, 509, 167
Carroll, S. M. 2001, LRR, 4, 1
Chaudhary, H., Capozziello, S., Praharaj, S., Pacif, S. K. J., & Mustafa, G. 2026, JHEAp, 50, 100507
Chaudhary, H., Capozziello, S., Sharma, V. K., Gómez-Vargas, I., & Mustafa, G. 2025b, arXiv:2508.10514
Chen, S.-F., Ivanov, M. M., Philcox, O. H. E., & Wenzl, L. 2024, PhRvL, 133, 231001
Chevallier, M., & Polarski, D. 2001, IJMPD, 10, 213
Cortês, M., & Liddle, A. R. 2025, MNRAS, 544, L121
Dawson, K., Hearin, A., Heitmann, K., et al. 2022, arXiv:2203.07291
De Bernardis, P., Ade, P. A., Bock, J. J., et al. 2000, Natur, 404, 955
De Felice, A., & Tsujikawa, S. 2010, LRR, 13, 1
Di Valentino, E. 2021, MNRAS, 502, 2065
Efstathiou, G. 1999, MNRAS, 310, 842
Efstathiou, G. 2025, MNRAS, 538, 875
Einstein, A. 1917, SPAW, 1917, 142
Fazzari, E., Giarè, W., & Di Valentino, E. 2025, ApJ, 996, L5
Foley, R., Scolnic, D., & Rest, A. 2018, MNRAS, 475, 193
Frieman, J. A., Turner, M. S., & Huterer, D. 2008, ARA&A, 46, 385
Gelman, A., & Rubin, D. B. 1992, StaSc, 7, 457
Gialamas, I. D., Hütsi, G., Kannike, K., et al. 2025, PhRvD, 111, 043540
Goliath, M., Amanullah, R., Astier, P., Goobar, A., & Pain, R. 2001, A&A, 380, 6
Guin, G., Paul, S., & Gangopadhyay, S. 2025, JCAP, 11, 048
Hastings, W. K. 1970, Biometrika, 57, 97
Heavens, A., Fantaye, Y., Mootoovaloo, A., et al. 2017, arXiv:1704.03472
Hicken, M., Challis, P., Jha, S., et al. 2009, ApJ, 700, 331
Hicken, M., Challis, P., Kirshner, R. P., et al. 2012, ApJS, 200, 12
Hinshaw, G., Weiland, J., Hill, R., et al. 2009, ApJS, 180, 225
Huang, L., Cai, R.-G., & Wang, S.-J. 2025, SCPMA, 68, 100413
Ivanov, M. M., Obuljen, A., Cuesta-Lazaro, C., & Toomey, M. W. 2025, PhRvD, 111, 063548
Jassal, H., Bagla, J., & Padmanabhan, T. 2005, MNRAS, 356, L11
Jiang, J.-Q., Pedrotti, D., da Costa, S. S., & Vagnozzi, S. 2024, PhRvD, 110, 123519
Jimenez, R., & Loeb, A. 2002, ApJ, 573, 37
Joudaki, S., Blake, C., Johnson, A., et al. 2018, MNRAS, 474, 4894
Karim, M. A., Aguilar, J., Ahlen, S., et al. 2025, arXiv:2503.14745
Kass, R. E., & Raftery, A. E. 1995, JASA, 90, 773
Komatsu, E., Dunkley, J., Nolta, M., et al. 2009, ApJS, 180, 330
Laurent, P., Le Goff, J.-M., Burtin, E., et al. 2016, JCAP, 11, 060
Lee, S. 2025, arXiv:2507.01380
Lee, S. 2026, EPJC, 86, 191
Lewis, A. 2025, JCAP, 2025, 025
Li, M., Li, X.-D., Wang, S., & Wang, Y. 2011, CoTPh, 56, 525
Li, T.-N., Du, G.-H., Zhou, S.-H., et al. 2026, PDU, 52, 102254
Li, X., & Shafieloo, A. 2019, ApJL, 883, L3
Li, X., & Shafieloo, A. 2020, ApJ, 902, 58
Linder, E. V. 1988, A&A, 206, 175
Linder, E. V. 2003, PhRvL, 90, 091301
Liu, T., Li, X., Xu, T., Biesiada, M., & Wang, J. 2025, EPJC, 85, 1351
Lodha, K., Calderon, R., Matthewson, W., et al. 2025a, PhRvD, 112, 083511
Lodha, K., Shafieloo, A., Calderon, R., et al. 2025b, PhRvD, 111, 023532
Mangano, G., Miele, G., Pastor, S., & Peloso, M. 2002, PhLB, 534, 8
Mazumdar, R., Gohain, M. M., & Bhuyan, K. 2025, arXiv:2507.05975
Moresco, M. 2015, MNRAS, 450, L16
Moresco, M., Cimatti, A., Jimenez, R., et al. 2012, JCAP, 2012, 006
Moresco, M., Jimenez, R., Verde, L., Cimatti, A., & Pozzetti, L. 2020, ApJ, 898, 82
Moresco, M., Jimenez, R., Verde, L., et al. 2018, ApJ, 868, 84
Moresco, M., Pozzetti, L., Cimatti, A., et al. 2016, JCAP, 2016, 014
Najafi, M., Pan, S., Di Valentino, E., & Firouzjaee, J. T. 2024, PDU, 45, 101539
Nojiri, S., Odintsov, S. D., & Oikonomou, V. K. 2017, PhR, 692, 1
Padmanabhan, T. 2003, PhR, 380, 235
Park, C.-G., de Cruz Pérez, J., & Ratra, B. 2025, IJMPD, 34, 2550058
Pedrotti, D., Escamilla, L. A., Marra, V., Perivolaropoulos, L., & Vagnozzi, S. 2026, PhRvD, 113, 043507
Perlmutter, S., Aldering, G., Goldhaber, G., et al. 1999, ApJ, 517, 565
Piedipalumbo, E., Vignolo, S., Feola, P., & Capozziello, S. 2023, PDU, 42, 101274
Popovic, B., Shah, P., Kenworthy, W., et al. 2025, arXiv:2511.07517
Roy Choudhury, S. 2025, ApJL, 986, L31
Roy Choudhury, S., & Okumura, T. 2024, ApJL, 976, L11
Roy Choudhury, S., Okumura, T., & Umetsu, K. 2025, ApJL, 994, L26
Riess, A. G., Filippenko, A. V., Challis, P., et al. 1998, AJ, 116, 1009
Rubin, D., Aldering, G., Betoule, M., et al. 2025, ApJ, 986, 231
Sahni, V., & Starobinsky, A. 2006, IJMPD, 15, 2105
Scrimgeour, M. I., Davis, T., Blake, C., et al. 2012, MNRAS, 425, 116
Sharma, V. K., Chaudhary, H., & Kolekar, S. 2026, JHEAp, 51, 100518
Silva, R., Goncalves, R., Alcaniz, J., & Silva, H. 2012, A&A, 537, A11
Sotiriou, T. P., & Faraoni, V. 2010, RvMP, 82, 451
Spergel, D., Gehrels, N., Baltay, C., et al. 2015, arXiv:1503.03757
Vagnozzi, S. 2020, PhRvD, 102, 023518
Vagnozzi, S. 2023, Univ, 9, 393
Vagnozzi, S., Loeb, A., & Moresco, M. 2021, ApJ, 908, 84
Weinberg, S. 1987, PhRvL, 59, 2607
Weinberg, S. 1989, RvMP, 61, 1
Wu, P.-J., & Zhang, X. 2025, PhRvD, 112, 063514
Ye, G., Martinelli, M., Hu, B., & Silvestri, A. 2025, PhRvL, 134, 181002
Zel'dovich, Y. B. 1968, SvPhU, 11, 381